CP3-Origins-2012-22
DIAS-2012-23

The Higgs boson and Top quark masses as tests of Electroweak Vacuum Stability

Isabella Masina[a,b]

[a] *Dipartimento di Fisica dell'Università di Ferrara and INFN Sezione di Ferrara, Via Saragat 1, I-44100 Ferrara, Italy*

[b] *CP^3-Origins and DIAS, Southern Denmark University, Campusvej 55, DK-5230 Odense M, Denmark*

The measurements of the Higgs boson and top quark masses can be used to extrapolate the Standard Model Higgs potential at energies up to the Planck scale. Adopting a NNLO renormalization procedure, we: i) find that electroweak vacuum stability is at present allowed, discuss the associated theoretical and experimental errors and the prospects for its future tests; ii) determine the boundary conditions allowing for the existence of a shallow false minimum slightly below the Planck scale, which is a stable configuration that might have been relevant for primordial inflation; iii) derive a conservative upper bound on type I seesaw right-handed neutrino masses, following from the requirement of electroweak vacuum stability.

I. INTRODUCTION

The recent discovery of a particle consistent with the Standard Model (SM) Higgs boson, announced by the ATLAS [1] and CMS [2] collaborations at CERN, is a milestone in particle physics; adding in quadrature statistical and systematic errors, the mass of the particle turns out to be in the range $124.8 - 126.5$ GeV at 2σ.

Here we assume that the new particle is actually the SM Higgs boson and study the implications that its mass value, together with other relevant parameters such as the top

quark mass and the strong gauge coupling, have on the behavior of the Higgs potential at very high energy scales and, in particular, for the sake of electroweak vacuum stability.

The project of extrapolating the Higgs potential up to the Planck scale is a long standing one [3–5], and was revamped in the fall of 2011 [6–9] after the first LHC hints of a Higgs boson [10]. Recently, the tools for a Next-to-Next-to-Leading Order (NNLO) renormalization procedure were derived [11–14]. So, there are now all the ingredients to carry on this long standing project. Clearly, the extrapolation is based on the assumption that there is a desert up to the Planck scale or, better, that possible new physics do not affect significantly the running of the Higgs quartic coupling, dominating the Higgs potential at high energy.

It is interesting that the recently discovered experimental Higgs mass range, combined with the experimental top mass range, indicates a particularly intriguing high energy behavior of the Higgs potential, close to the transition between electroweak vacuum stability and metastability. This is due to the fact that, for these Higgs and top mass values, the Higgs quartic coupling can be very small or even negative. Since the dependence on the top mass is strong and quite subtle, it is not surprising that different groups slightly disagree in the interpretation of the results, some of them favoring [13] and some other disfavoring [14] electroweak vacuum stability.

Traditionally the top pole mass was used in the analysis, but it has been pointed out [15] that the top pole mass value used in previous analyses and taken to be the one measured at Tevatron, $m_t^{exp} = 173.2 \pm 0.9$ GeV [16], is not unambiguously derived and that a more careful derivation should be rather based on the running top mass in the $\overline{\rm MS}$ scheme, $\overline{m_t}(m_t) = 163.3 \pm 2.7$ GeV. As shown in [15], the top pole mass range consistently derived from the running one, $m_t = 173.3 \pm 2.8$ GeV, is plagued by a larger error than the Tevatron measurement considered in [14], rescuing electroweak vacuum stability.

In our analysis we keep as a free parameter the running top mass, rather than the pole one. In this way we completely avoid the theoretical uncertainties associated to the top Yukawa matching procedure. As we are going to discuss, the theoretical error associated to the Higgs quartic coupling matching [13, 14] turns out to be smaller than the one induced by the experimental uncertainty on the strong gauge coupling, $\alpha_3(m_Z)$. Given the above mentioned range for the running top mass [15], we find that electroweak stability is allowed in the whole Higgs mass range [1, 2]. Stability could be soon excluded if values of the running top mass $\overline{m_t}(m_t) < 163$ GeV could be excluded by the LHC. Otherwise, testing electroweak vacuum stability would become very challenging, since this would require precision measurements of the Higgs and top masses, and also of $\alpha_3(m_Z)$.

A stable Higgs potential configuration which deserves particular interest is a shallow false minimum close to the Planck scale, which could have been relevant for primordial inflation [7, 17, 18]. We show that such configuration is realized only if the Higgs quartic coupling and its derivative satisfy very specific boundary conditions, possibly having a

deep origin in quantum gravity.

As well know, new physics in addition to the SM is required to explain neutrino masses and mixings, and also dark matter. The mechanism responsible for neutrino masses could affect the Higgs quartic coupling; as an example, we consider the impact that the inclusion of neutrino masses via a type I seesaw has on electroweak stability, discussing in some detail the shallow false minimum configuration.

The paper is organized as follows. In sec. II we discuss the input parameters and the NNLO renormalization procedure used to extrapolate the Higgs potential up to the Planck scale. An analysis of electroweak vacuum stability and the associated constraints on the top and Higgs masses, with a detailed discussion of the theoretical errors and the prospects for the future, are presented in sec. III. In sec. IV we investigate the boundary conditions leading to the particularly interesting configuration of a shallow false minimum below the Planck scale. Sec. V is devoted to the upper bound on the seesaw right-handed neutrino masses following from the requirement of electroweak vacuum stability. Conclusions are drawn in sec. VI. Appendix A contains the relevant formulas for the NNLO running procedure in the SM and, in appendix B, those to incorporate the type I seesaw mechanism.

II. INPUT PARAMETERS AND RENORMALIZATION AT NNLO

The normalization of the Higgs quartic coupling λ is chosen in this paper so that the potential for the physical Higgs ϕ_H contained in the Higgs doublet $H = (0, (\phi_H + v)/\sqrt{2})$ is given, at tree level, by

$$V(\phi_H) = \frac{\lambda}{6}\left(|H|^2 - \frac{v^2}{2}\right)^2 \approx \frac{\lambda}{24}\phi_H^4 \quad , \tag{1}$$

where $v = 1/(\sqrt{2}G_\mu)^{1/2} = 246.221$ GeV and $G_\mu = 1.1663787(6) \times 10^{-5}/\text{GeV}^2$ is the Fermi constant from muon decay [19]. The approximation in eq. (1) holds when considering large field values. According to our normalization, the physical Higgs mass satisfies the tree level relation $m_H^2 = \lambda v^2/3$. In addition, the mass of the fermion f reads, at tree level, $m_f = h_f v/\sqrt{2}$, where h_f denotes the associated Yukawa coupling.

In order to extrapolate the behavior of the Higgs potential at very high energies, we adopt the $\overline{\text{MS}}$ scheme and consider the Renormalization Group (RG) evolution for the relevant couplings which, in addition to the Higgs quartic coupling λ, are the gauge g, g', g_3, and the top Yukawa h_t couplings. We work at NNLO, namely 3-loops for the β-functions and 2-loops for the matching conditions at some suitable scale.

It is customary to introduce the dimensionless parameter $t = \log \mu/m_Z$, where μ stands for the renormalization scale and m_Z is the Z boson mass. The RG equations for the

relevant couplings are then given by

$$\begin{aligned}
\frac{d}{dt}\lambda(t) &= \kappa\beta_\lambda^{(1)} + \kappa^2\beta_\lambda^{(2)} + \kappa^3\beta_\lambda^{(3)} \,, \\
\frac{d}{dt}h_t(t) &= \kappa\beta_{h_t}^{(1)} + \kappa^2\beta_{h_t}^{(2)} + \kappa^3\beta_{h_t}^{(3)} \,, \\
\frac{d}{dt}g(t) &= \kappa\beta_g^{(1)} + \kappa^2\beta_g^{(2)} + \kappa^3\beta_g^{(3)} \,, \\
\frac{d}{dt}g'(t) &= \kappa\beta_{g'}^{(1)} + \kappa^2\beta_{g'}^{(2)} + \kappa^3\beta_{g'}^{(3)} \,, \\
\frac{d}{dt}g_3(t) &= \kappa\beta_{g_3}^{(1)} + \kappa^2\beta_{g_3}^{(2)} + \kappa^3\beta_{g_3}^{(3)} \,,
\end{aligned} \tag{2}$$

where $\kappa = 1/(16\pi^2)$ and the apex on the β-functions represents the loop order. The 1-loop and 2-loop expressions for the β-functions can be found *e.g.* in ref. [20] (see also [21–26]). Recently, the complete 3-loop β-functions for all the SM gauge couplings have been presented by Mihaila, Salomon and Steinhauser in ref. [11], while the leading 3-loop terms in the RG evolution of λ, h_t and the Higgs anomalous dimension have been computed by Chetyrkin and Zoller in ref. [12]. For the sake of completeness, the expressions for the β-functions up to 3-loops are collected in appendix A.

The matching of the running gauge couplings is done at the Z boson pole mass, m_Z. The numerical values used for the related $\overline{\rm MS}$ observables are taken from the latest Particle Data Group SM fit results [19]:

$$\begin{aligned}
\alpha_{em}^{-1}(m_Z) = 127.944 \pm 0.014 \;,\;\; \alpha_3(m_Z) = 0.1196 \pm 0.0017 \;, \\
\sin^2\theta_W(m_Z) = 0.23116 \pm 0.00012 \;,\;\; m_Z = 91.1874 \pm 0.0021 \text{ GeV} \;.
\end{aligned} \tag{3}$$

To match the $\overline{\rm MS}$ running quartic coupling $\lambda(\mu)$ with the Higgs pole mass m_H is more complicated and requires to exploit an expansion,

$$\lambda(\mu) = \sum_{n=1,2,3,\ldots} \lambda^{(n)}(\mu) = 3\frac{m_H^2}{v^2}\left(1 + \delta_H^{(1)}(\mu) + \delta_H^{(2)}(\mu) + \ldots\right) \,, \tag{4}$$

which is know at present at NLO: $\delta_H^{(1)}(\mu)$ is the 1-loop $\mathcal{O}(\alpha)$ result of Sirlin and Zucchini [27] while $\delta_H^{(2)}(\mu)$ is the recently calculated 2-loop result, composed by a QCD contribution of $\mathcal{O}(\alpha\alpha_3)$ [13, 14] and a Yukawa contribution [14]. More details can be found in appendix A. As well known, there is some arbitrariness in the choice of the matching scale μ in eq. (4), which introduces a "theoretical" error in the RG procedure. In this work, we choose to perform the matching of the Higgs quartic coupling λ at the scale $\mu = m_H$. The theoretical uncertainty is estimated by performing the matching also at different scales and by evolving λ via RG running until $\mu = m_H$. The spread in the numerical values obtained for $\lambda(m_H)$ can then be used to infer the magnitude of the theoretical error.

This is illustrated in fig. 1, assuming for definiteness a top pole mass $m_t = 172\,\text{GeV}$. The dashed and solid curves show the value of $\lambda(m_H)$ obtained by including the corrections up

to 1-loop and 2-loop respectively, for various choices of the matching scale: from top to bottom $\mu = m_Z$, m_H, m_t, $2m_H$. One can see that, working at the 1-loop, the theoretical uncertainty is about 5%. The inclusion of the 2-loop corrections given in ref. [14] reduces the theoretical uncertainty down to about 0.7%. Notice also that the preferred region shrinks to small λ values and that $\mu = m_Z$ and $\mu = m_H$ nearly overlap. More generally, one can use the following expression for the 2-loop result,

$$\lambda(m_H) = 0.8065 + 0.0109\,(m_H[\text{GeV}] - 126) + 0.0015\,(m_t[\text{GeV}] - 172)\,{}^{+0.0002}_{-0.006}\,, \qquad (5)$$

where the mean value refers to $\mu = m_H$.

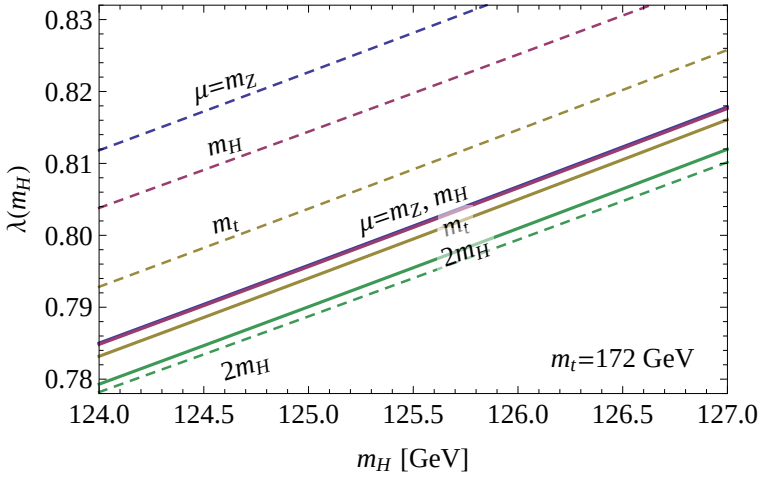

FIG. 1: Value of $\lambda(m_H)$ obtained by performing the matching at different scales μ, indicated by the labels, as a function of m_H. The solid (dashed) lines are obtained by including corrections up to 2-loop (1-loop). We fixed $m_t = 172$ GeV (for different values see eq.(5)).

It is common to extrapolate the $\overline{\text{MS}}$ top Yukawa coupling $h_t(\mu)$ from the matching condition between the running top mass $\overline{m_t}(\mu)$ and the top pole mass m_t:

$$h_t(\mu)\frac{v}{\sqrt{2}} = \overline{m_t}(\mu) = m_t\Big(1 + \delta_t(\mu)\Big)\,, \quad \delta_t(\mu) = \delta_t^W(\mu) + \delta_t^{QED}(\mu) + \delta_t^{QCD}(\mu)\,, \qquad (6)$$

where $\delta_t^W + \delta_t^{QED}$ represent the electroweak contribution, which is known at 1-loop [28], while δ_t^{QCD} is the QCD one. The QCD 1-loop result is known since many years [28]; the QCD 2-loop and 3-loop results as a function of the matching scale μ are given in [29] (see also [30–34]). The matching is usually done at the top pole mass scale, and the theoretical error associated to the arbitrariness of the matching scale can be estimated as before, namely by comparing the values of $h_t(m_t)$ obtained with different matching scales. This is represented in fig. 2, where the curves are obtained by working at 2-loop

and using, from bottom to top, $\mu = m_Z, m_t, 2m_t$. The plot shows that the associated theoretical uncertainty is about 2%. The analytical expression for $h_t(m_t)$ is:

$$h_t(m_t) = 0.933 + 0.006\,(m_t[\text{GeV}] - 172)\,^{+0.017}_{-0.013}\,. \tag{7}$$

The procedure adopted in previous analyses of the stability of the electroweak vacuum was to use the experimental value of m_t, identified with the one measured at the Tevatron by the CDF and D0 collaborations, $m_t^{exp} = 173.2 \pm 0.9$ GeV [16], to extrapolate the running Yukawa $h_t(m_t)$ via eq. (7). However, as discussed in ref. [15], it is not meaningful to use the mass parameter provided by the Tevatron as the pole top mass to be inserted in eq. (7): the running top mass in the $\overline{\text{MS}}$ scheme is instead a well defined parameter that can be directly extracted at NNLO from Tevatron measurements of the inclusive top pair production cross-section, giving $\overline{m_t}(m_t) = 163.3 \pm 2.7$ GeV [15]. So, it is conceptually more robust and practically more convenient to extract the top Yukawa coupling directly from $\overline{m_t}(m_t)$, as will be done in the following[1]. Our results will thus be presented as a function of $\overline{m_t}(m_t)$.

Notice that, according to eq. (7), the value of the top pole mass can be easily recovered via the relation $m_t = \overline{m_t}(m_t) + 9.6\,^{+2.9}_{-2.3}$ GeV, which however is plagued by a large

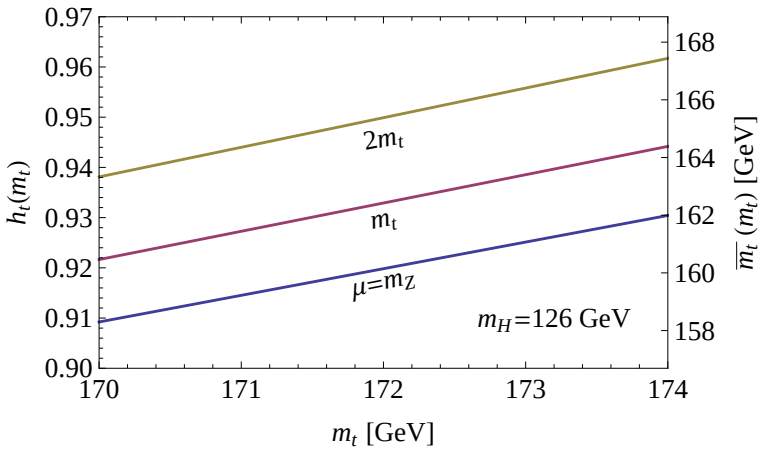

FIG. 2: Values of $h_t(m_t)$ and $\overline{m_t}(m_t)$ as a function of m_t. The curves are obtained by matching at different scales, which are indicated by the labels. We fixed $m_H = 126$ GeV for definiteness but the results do not significantly dependent on m_H, provided it is chosen in its experimental range.

[1] At difference, ref. [15] proceeds in a more complicated way: the value of $\overline{m_t}(m_t)$ is translated into a value of m_t, to be inserted in the expression of the lower bound on m_H ensuring electroweak vacuum stability as derived in ref. [14].

uncertainty. In ref. [15] it was found that, by doing a scheme transformation to NNLO accuracy from the running to the pole top mass, the range $\overline{m_t}(m_t) = 163.3 \pm 2.7$ GeV is equivalent to $m_t = 173.3 \pm 2.8$ GeV. Hence, while displaying our results as a function of $\overline{m_t}(m_t)$ as already stated, motivated by the results of ref. [15], in some plots (as the one in fig. 5) we will link the value of the top pole mass to the running mass via the simple relation $m_t = \overline{m_t}(m_t) + 10$ GeV.

Before presenting the results of our analysis in the following sections, we recall that, in order to carefully study the shape of the Higgs potential at high energy, one should consider the renormalization improved effective potential. This can be done by introducing an effective coupling, $\lambda_{eff}(\mu) = \lambda(\mu) + \Delta\lambda(\mu)$, so that

$$V_{eff}(\phi_H) = \frac{\lambda_{eff}(\mu)}{24}\phi_H^4 \ . \tag{8}$$

The expression for $\Delta\lambda(\mu)$ is known up to 2-loop [4, 20] (and given, for instance, in [14]). Since the scalar contribution is not well defined when λ is negative, in the following we consider the renormalization improved potential at the tree level, and identify μ with ϕ_H. It is well known that this simplification has a negligible impact in the determination of the vacuum stability bound to be discussed in the next section.

III. ELECTROWEAK VACUUM STABILITY

The experimental region of the values of the Higgs and top masses is very intriguing form the theoretical point of view, since the Higgs quartic coupling could be rather small, vanish or even turn negative at a scale slightly smaller than the Planck scale. Accordingly, the behavior of the Higgs potential at high energy changes drastically: if $\lambda(\mu)$ is always positive, the electroweak vacuum is a global minimum, possibly accompanied by another local minimum just below the Planck scale, which could have played a role in primordial inflation [7, 17, 18]; if $\lambda(\mu)$ turns negative below $M_{\rm Pl}$, the electroweak vacuum correspondingly becomes metastable [4, 5].

These drastically different possibilities for the behavior of the renormalization improved Higgs potential at high energy are illustrated in the left plot fig. 3, where $m_H = 126\,\text{GeV}$ and some specific values for $\overline{m_t}(m_t)$ have been selected, increasing from top to bottom. The right plot shows the associated values of $\lambda(\mu)$. Let start considering the value $\overline{m_t}(m_t) = 161.989$ GeV. Increasing the latter by just 1 MeV, the potential develops an inflection point; notice that the associated $\lambda(\mu)$ becomes as small as $\mathcal{O}(10^{-5})$. Increasing again $\overline{m_t}(m_t)$ by about 200 keV, the minimum of $\lambda(\mu)$ is equal to zero: a second vacuum degenerate with the electroweak one is obtained. Further increasing $\overline{m_t}(m_t)$ makes $\lambda(\mu)$ turn negative: the electroweak vacuum becomes metastable.

The dashed curve in the right plot in fig. 3 shows the evolution of $\beta_\lambda(\mu) = d\lambda(\mu)/dt$

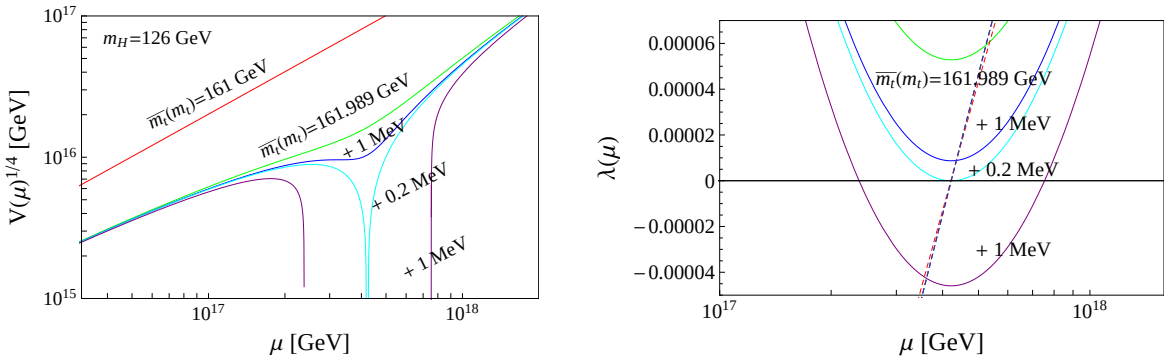

FIG. 3: The SM Higgs potential (left) and the quartic Higgs coupling (right) as functions of the renormalization scale μ, for $m_H = 126$ GeV and different values of $\overline{m_t}(m_t)$, increasing from top to bottom by the amount indicated by the labels. The dashed curve in the right plot shows the associated value of $\beta_\lambda(\mu)$. The other input parameters are fixed at the central values discussed in the previous section.

for the same parameter values; there is only a single dashed curve because $\beta_\lambda(\mu)$ mildly depends on $\overline{m_t}(m_t)$ if the latter is in the range $161 - 163$ GeV. Let call μ_β the renormalization scale such that $\beta_\lambda(\mu_\beta) = 0$. Clearly, only in the case of two degenerate vacua the conditions $\beta_\lambda(\mu_\beta) = 0$ and $\lambda(\mu_\beta) = 0$ are simultaneously met. For a shallow false minimum we instead have $\beta_\lambda(\mu_\beta) = 0$ and $\lambda(\mu_\beta) = \mathcal{O}(10^{-5})$, as already mentioned.

In fig. 4 we show how μ_β depends on $\overline{m_t}(m_t)$, for various values of m_H. It is remarkable that μ_β is maximized and nearly constant for the values of $\overline{m_t}(m_t)$ for which $\lambda(\mu)$ is very small.

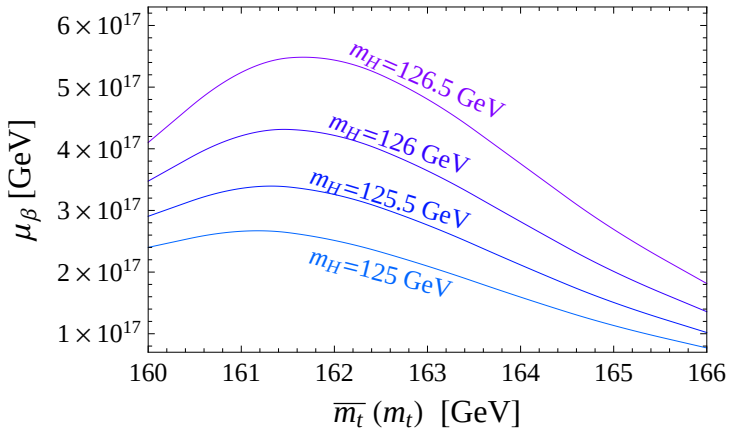

FIG. 4: The scale μ_β as a function of $\overline{m_t}(m_t)$ and for different values of m_H, as indicated by the labels.

We now turn to the determination of the points in the plane $[m_H, \overline{m_t}(m_t)]$ allowing for the existence of a second minimum degenerate with the electroweak one. These points belong to a line separating the stability from the metastability region, see fig. 5: in the lower part of the plot $\lambda(\mu)$ is always positive, while in the upper part it becomes negative before reaching the Planck scale. The configuration of a shallow false minimum belongs to the stability region, but the associated points are so close to the transition line that they could not be distinguished by eye.

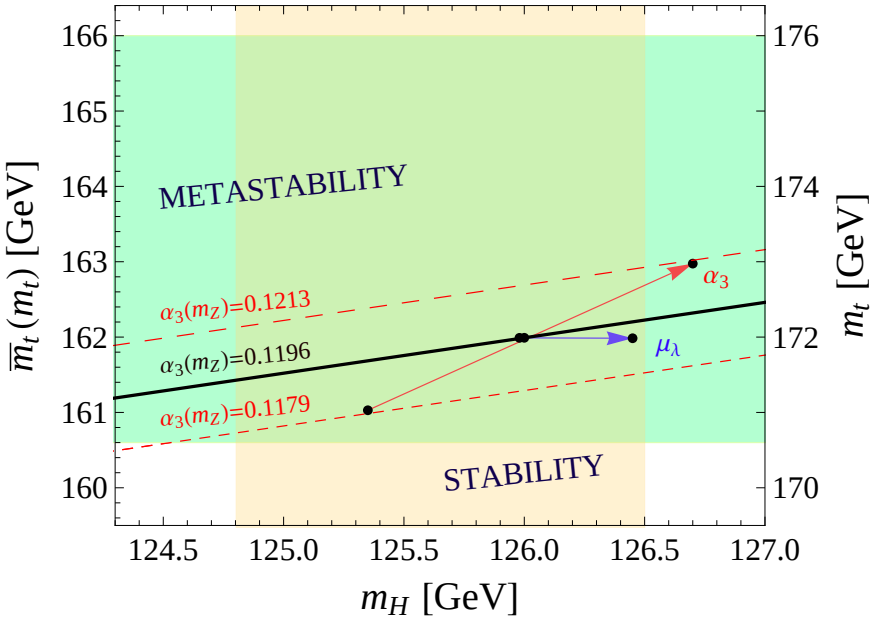

FIG. 5: The solid (black) line marks the points in the plane $[m_H, \overline{m_t}(m_t)]$ where a second vacuum, degenerate with the electroweak one, is obtained just below the Planck scale. The (red) diagonal arrow shows the effect of varying $\alpha_3(m_Z) = 0.1196 \pm 0.0017$; the (blue) horizontal one shows the effect of varying μ_λ (the matching scale of λ) from m_Z up to $2m_H$. The shaded (yellow) vertical region is the 2σ ATLAS [1] and CMS [2] combined range, $m_H = 125.65 \pm 0.85$ GeV; the shaded (green) horizontal region is the range $\overline{m_t}(m_t) = 163.3 \pm 2.7$ GeV, equivalent to $m_t = 173.3 \pm 2.8$ GeV [15].

The transition line of fig. 5 was obtained with the input parameter values discussed in the previous section and by matching the running Higgs quartic coupling at m_H. Clearly, it is also important to estimate the theoretical error associated to experimental ranges of the input parameters and the one associated to the matching procedure. To illustrate this, we consider in particular the point on the transition line associated to the value $m_H = 126$ GeV; for such point, λ and β_λ both vanish at a certain scale μ_β (see fig. 4). The arrows show how, if some inputs or the matching scale are changed, the position of this point

have to change in order to keep having, at the same scale μ_β, a vacuum degenerate with the electroweak one. The diagonal arrow is obtained by varying the strong coupling in its allowed range, $\alpha_3(m_Z) = 0.1196 \pm 0.0017$; the short (long) dashed line shows how the solid line would move if $\alpha_3(m_Z)$ were equal to its minimum (maximum) presently allowed value. Notice that the error on $\alpha_3(m_Z)$ induces an uncertainty in both the Higgs and top masses of about ± 0.7 GeV. The variation of the other input parameters induces a much smaller effect. The horizontal arrow is instead obtained by varying μ_λ, the matching scale of the Higgs quartic coupling, from $\mu = m_Z$ to $\mu = 2m_H$; notice that the associated error is very asymmetric (see fig. 1): essentially it can only enhance m_H, by at most 0.5 GeV. Clearly, similar considerations apply to each point of the transition line.

Since stability can be achieved in the whole experimental range for m_H (shaded vertical region), but this is not the case for $\overline{m_t}(m_t)$ (shaded horizontal region), it is more convenient to write down the condition of electroweak vacuum stability under the form of an upper bound on the top mass:

$$\overline{m_t}(m_t)[\text{GeV}] \leq 162.0 + 0.47\,(m_H[\text{GeV}] - 126) \pm 0.7_{\alpha_3} - 0.2_{\mu_\lambda} \ . \tag{9}$$

The first error is associated to the experimental error on $\alpha_3(m_Z)$, while the second accounts for the theoretical error induced by the matching of λ. Since the latter is smaller and can be easily accounted for by just shifting m_H upwards by at most 0.5 GeV, it will not be explicitly shown in the following plots.

Given the present experimental situation, in order to understand whether we live in a stable or metastable vacuum it is crucial to better determine $\overline{m_t}(m_t)$. As discussed in [15], after LHC the Higgs mass will presumably be known with an accuracy of $\mathcal{O}(100)$ MeV [35], but the precision on the top mass would improve only by a factor of two. For instance, if the whole range of $\overline{m_t}(m_t)$ below 163 GeV would be excluded, we would conclude that our vacuum is metastable; otherwise the investigations should continue.

A self-consistent and precise determination of the top quark mass can best be performed at a high-energy electron-positron collider, with a planned accuracy of $\mathcal{O}(100)$ MeV. Moreover, at an electron-positron collider $\alpha_3(m_Z)$ could be determined with an accuracy close to or better than $\Delta\alpha_3(m_Z) = 0.0007$ (this precision is sometimes currently adopted [13, 14] but cannot be considered to be conservative according to ref. [15]). At this stage, if the stability region will still have an overlap with the allowed ranges of the top and Higgs masses, we will be mostly limited by the theoretical uncertainty associated to μ_λ.

Notice also that it is not realistic to hope to distinguish the case of two degenerate minima with the one of a shallow false minimum, since the difference in the top mass is just about 200 keV (see fig. 3).

IV. SHALLOW FALSE MINIMUM

It is interesting to study in some detail the boundary conditions which must be satisfied in order to have a very shallow false minimum just below the Planck scale, since it could be relevant for inflation [7, 17, 18].

To study this particular configuration, we denote with μ_i the renormalization scale where the Higgs potential has an inflection point; we also recall that μ_β has been defined to be the scale where $\lambda(\mu_\beta) = 0$ and $\beta_\lambda(\mu_\beta) = 0$ are simultaneously fulfilled. Both μ_i and μ_β increase[2] with m_H, as shown in fig. 6, where the shaded region accounts for the experimental range of $\alpha_3(m_Z)$.

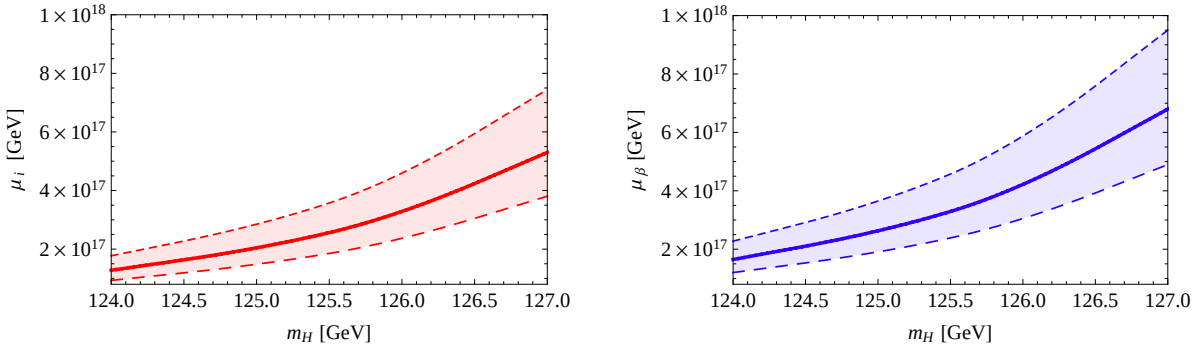

FIG. 6: Values of μ_i (left) and μ_β (right) as a function of m_H. For the solid lines, the input parameters are fixed at their central values and the matching of λ is done at $\mu = m_H$. The shaded regions shows the uncertainty induced by the experimental error of $\alpha_3(m_Z) = 0.1196 \pm 0.0017$: the short and long dashed curves refer to the lower and upper value at 1σ, respectively.

It is interesting that, for the whole experimental range of m_H, a shallow false minimum is obtained only if the following boundary condition holds:

$$\lambda(\mu_\beta) \simeq (8.75 \pm 0.15) \times 10^{-6} \quad . \tag{10}$$

One could speculate that such a special value could be dictated by an eventual merging with quantum gravity [6, 36]. In the left plot of fig. 7 we show that $\lambda(\mu_\beta)$ has a mild dependence on m_H; in the right plot we show instead the value of the Higgs potential at the inflection point, which turns out to be of $\mathcal{O}(10^{16})$ GeV. As before, the shaded regions account for the experimental range of $\alpha_3(m_Z)$.

As pointed out in [17], a way of testing the hypothesis that inflation occurred when the Higgs field was trapped into a shallow false vacuum below the Planck scale is to look

[2] Notice that μ_i is slightly smaller than μ_β. This can be easily understood, since the condition for having an inflection point at μ_i reads $\beta_\lambda(\mu_i) = -4\lambda(\mu_i) < 0$, which implies $\mu_i < \mu_\beta$.

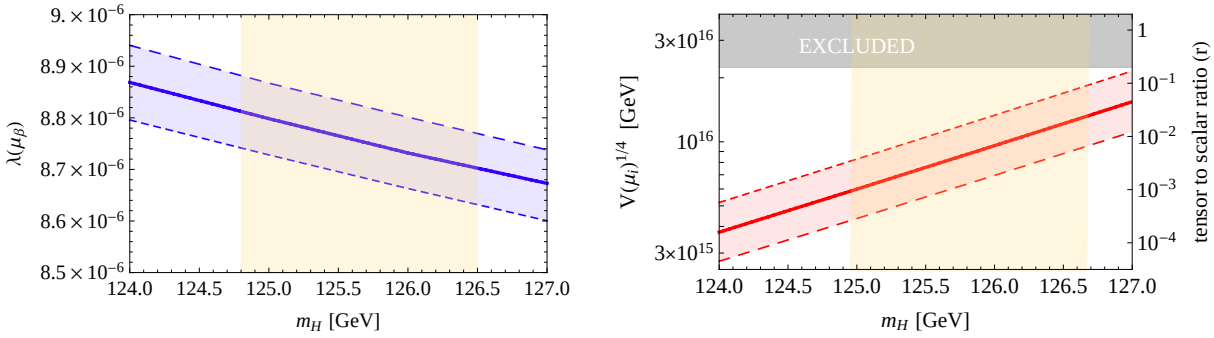

FIG. 7: Left: the value of $\lambda(\mu_\beta)$ as a function of m_H. Right: the Higgs potential at μ_i and the associated prediction for r as a function of m_H. The short and long dashed curves refer to the 1σ lower and upper values of $\alpha_3(m_Z)$, respectively. The shaded (yellow) vertical region marks the preferred range of m_H at 2σ [1, 2]. The upper region in the right plot is excluded because $r \lesssim 0.2$ [37].

at the tensor-to-scalar ratio r of cosmological perturbations. The amplitude of density fluctuations in the observed Universe as seen by the CMB and Large-Scale structure data is parametrized by the power spectrum in k-space, $P_s(k) = \Delta^2_R\,(k/k_0)^{n_S-1}$, where Δ^2_R is the amplitude at some pivot point k_0, whose best-fit value is $\Delta^2_R = (2.43 \pm 0.11) \times 10^{-9}$ at $k_0 = 0.002\,\mathrm{Mpc}^{-1}$ [37]. In models where inflation happened while the Higgs was trapped in the shallow minimum [7, 18], the Higgs potential at the inflection point and the amount of gravity waves that can be produced - parametrized via the tensor-to-scalar ratio r - are linked via a simple relation:

$$\Delta^2_R = \frac{2}{3\pi^2}\frac{1}{r}\frac{V(\mu_i)}{M^4}\ , \tag{11}$$

where M is the reduced Planck scale. Such prediction for r is reported in the right plot of fig. 7. Notice that, for these models, only if m_H is in its upper allowed range and $\alpha_3(m_Z)$ is quite low, there are chances for the Planck satellite mission [38] to measure r. However, the forthcoming experiment EPIC [39] should be able to test r down to 10^{-2}, while COrE [40] down to about 10^{-3}.

V. CONSTRAINTS ON THE SEESAW MECHANISM

We now consider the effect of including neutrino masses via a type I seesaw. This issue has been already considered in a series of papers [8, 41–44].

Although the precise amount of the effect is quite model dependent, here we obtain a conservative estimate of the effect by considering only one right handed neutrino with mass M_ν, associated to a light Majorana neutrino with mass $m_\nu = 0.06$ eV, the scale of

the atmospheric oscillations. This is supported by the following argument.

It is well known that the β-function of the Higgs quartic coupling is affected only if $h_\nu(\mu)$, the Yukawa coupling of the Dirac mass term (defined only for $\mu \geq M_\nu$), is large enough. As the top Yukawa coupling, also the neutrino Yukawa coupling induces a suppression of the Higgs quartic coupling at high energy. By increasing M_ν and m_ν, the neutrino Yukawa coupling at the threshold scale M_ν also increases:

$$h_\nu(M_\nu) = 2\sqrt{\frac{m_\nu(M_\nu)\, M_\nu}{v^2}} \ . \tag{12}$$

This justifies that the fact that we equate m_ν to the the atmospheric mass scale, about 0.06 eV, which is the lowest possible value for the heaviest among the three light neutrinos. In addition, two other Majorana neutrinos with masses lighter than m_ν can be accommodated via the seesaw but, if their right-handed neutrinos are lighter than M_ν, the associated Dirac Yukawa couplings are naturally expected to be smaller, and their effect on $\lambda(\mu)$ negligible.

In Appendix B we provide the additional terms (with respect to the pure SM) for the relevant β-functions, above and below the scale M_ν.

Since the effect of h_ν is a suppression of λ, a configuration with a stable electroweak vacuum in the SM, could be rendered metastable because of the addition of the seesaw interaction. For a fixed value of m_H, one can find the upper bound on M_ν following from the requirement that the electroweak vacuum is not destabilized. As shown in fig. 8 for $m_H = 126$ GeV (but similar upper bounds are obtained in the whole experimental

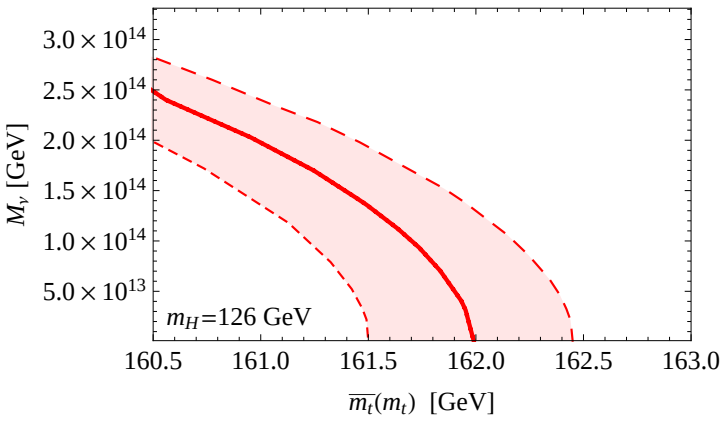

FIG. 8: Upper bound on M_ν as a function of the running top mass, following from the requirement that the electroweak vacuum is not destabilized because of the inclusion of the seesaw, for $m_H = 126$ GeV. The shaded region is obtained by varying $\alpha_3(m_Z)$ in its 1σ range.

range of m_H), such upper bound strongly depends on the top mass[3] and is affected by an uncertainty which is mainly due to $\alpha_3(m_Z)$ (shaded region). The smaller the top mass is, the more the configuration is stable and the less stringent is the M_ν upper bound, $M_\nu \lesssim 3 \times 10^{14}$ GeV. But increasing the top mass, the electroweak vacuum becomes less stable and the upper bound on M_ν becomes accordingly more and more stringent.

Let consider in particular the upper bound on M_ν needed to avoid destabilization of an inflection point configuration, as the one depicted via the dashed line in fig. 9. Notice that an inflection point becomes a not so shallow local second minimum if $M_\nu \sim 10^{11}$ GeV and that electroweak vacuum destabilization is avoided only if the condition $M_\nu \lesssim 2 \times 10^{11}$ GeV is satisfied. The latter bound might be relevant for models of inflation based on the SM shallow false minimum [7, 17, 18]; note however that it is well compatible with the thermal leptogenesis mechanism to explain matter-antimatter asymmetry, for which the lower bound on the lightest Majorana neutrino is about 5×10^8 GeV [45].

Clearly, the neutrino Yukawa coupling y_ν is not the only additional term beyond the SM capable of modifying the running of λ at high energy. Always in the context of type I seesaw, in the case that the vacuum expectation value of a singlet scalar field S (violating the lepton number by two units) is actually at the origin of the right-handed Majorana neutrino mass, the S couplings induce an enhancement of λ, thus helping the stability of

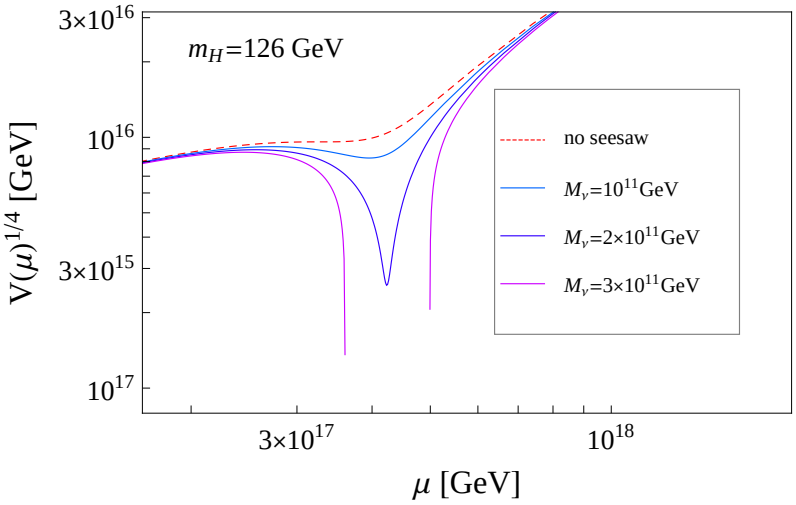

FIG. 9: The Higgs potential as function of the renormalization scale, for $m_H = 126$ GeV and a value of the top mass leading to an inflection point configuration in the SM case (dashed curve). The lower curves display the effect of adding the seesaw, with three increasing values of M_ν from top to bottom (solid curves).

[3] This dependence was not considered in the previous literature.

the electroweak vacuum [46]. Such effect is indeed generically expected when adding to the SM a singlet field S [46, 47].

VI. CONCLUSIONS

The recent discovery of a particle consistent with the SM Higgs boson [1, 2] provides a strong motivation to pursue [6–9, 13–15, 17] the old project [3–5] of investigating the behavior of the Higgs potential at very high energies. In particular, one would understand whether the electroweak vacuum is a global minimum up to the Planck scale, namely whether we live in a stable vacuum. In particular, a stable configuration which deserves a special interest is a shallow false minimum below the Planck scale: the Higgs field could have been primordially trapped there, leading to a stage of inflation [7, 17, 18]. Stability below the Planck scale is required also in Higgs inflation models with non minimal gravitational couplings [13, 48].

In our analysis, we adopted the recently derived tools for a NNLO renormalization procedure [11–14]. At difference of previous analyses, we considered as free parameter the running top mass rather than the (Tevatron) top pole mass, as suggested in ref. [15].

Given the present range of the running top mass and of the Higgs mass, we found that electroweak vacuum stability is at present allowed, as shown in fig. 5. To further test stability, a more precise measurement of the top mass would be crucial. As apparent from the stability condition of eq. (9), in case that LHC will not exclude values of the running top mass below 163 GeV, an electron-positron collider would probably be needed to discriminate between stability and metastability.

We also determined the high scale boundary conditions allowing for a shallow false minimum slightly below the Planck scale, $\lambda(\mu_\beta) \sim 10^{-5}$ (μ_β is the renormalization scale were the β-function of the Higgs quartic coupling vanishes), and discussed the prospects for the cosmological tests of such configuration.

Finally, a conservative upper bound on type I seesaw right-handed neutrino masses, following from the requirement of electroweak vacuum stability, was derived, analysing in particular its dependence on the top mass.

Acknowledgments

We would like to thank G. Isidori, A. Notari and A. Strumia for useful discussions.

Appendix A: Formulæ for the RG running at NNLO

1. The β-functions

Here we provide the expressions for the β-functions up to 3-loops, see eq. (2).
At 1-loop they are given by:

$$\begin{aligned}
\beta_\lambda^{(1)} &= \frac{27}{4}g(t)^4 + \frac{9}{2}g'(t)^2 g(t)^2 - 9\lambda(t)g(t)^2 + \frac{9}{4}g'(t)^4 - 36h_t(t)^4 + 4\lambda(t)^2 - 3g'(t)^2\lambda(t) \\
&\quad +12h_t(t)^2\lambda(t) \ , \\
\beta_{h_t}^{(1)} &= \frac{9}{2}h_t(t)^3 - \frac{9}{4}g(t)^2 h_t(t) - 8g_3(t)^2 h_t(t) - \frac{17}{12}g'(t)^2 h_t(t) \ , \\
\beta_g^{(1)} &= -\frac{19}{6}g(t)^3 \ , \\
\beta_{g'}^{(1)} &= \frac{41}{6}g'(t)^3 \ , \\
\beta_{g_3}^{(1)} &= -7g_3(t)^3 \ .
\end{aligned}$$

At 2-loop they are:

$$\begin{aligned}
\beta_\lambda^{(2)} &= 80g_3(t)^2 h_t(t)^2\lambda(t) - 192g_3(t)^2 h_t(t)^4 + \frac{915}{8}g(t)^6 - \frac{289}{8}g'(t)^2 g(t)^4 - \frac{27}{2}h_t(t)^2 g(t)^4 \\
&\quad -\frac{73}{8}\lambda(t)g(t)^4 - \frac{559}{8}g'(t)^4 g(t)^2 + 63g'(t)^2 h_t(t)^2 g(t)^2 + \frac{39}{4}g'(t)^2\lambda(t)g(t)^2 - 3h_t(t)^4\lambda(t) \\
&\quad +\frac{45}{2}h_t(t)^2\lambda(t)g(t)^2 - \frac{379}{8}g'(t)^6 + 180h_t(t)^6 - 16g'(t)^2 h_t(t)^4 - \frac{26}{3}\lambda(t)^3 - \frac{57}{2}g'(t)^4 h_t(t)^2 \\
&\quad -24h_t(t)^2\lambda(t)^2 + 6\left(3g(t)^2 + g'(t)^2\right)\lambda(t)^2 + \frac{629}{24}g'(t)^4\lambda(t) + \frac{85}{6}g'(t)^2 h_t(t)^2\lambda(t) \ ,
\end{aligned}$$

$$\begin{aligned}
\beta_{h_t}^{(2)} &= h_t(t)\left[-108g_3(t)^4 + 9g(t)^2 g_3(t)^2 + \frac{19}{9}g'(t)^2 g_3(t)^2 + 36h_t(t)^2 g_3(t)^2 - \frac{3}{4}g'(t)^2 g(t)^2 \right. \\
&\quad \left. -\frac{23}{4}g(t)^4 + \frac{1187}{216}g'(t)^4 - 12h_t(t)^4 + \frac{\lambda(t)^2}{6} + h_t(t)^2\left(\frac{225}{16}g(t)^2 + \frac{131}{16}g'(t)^2 - 2\lambda(t)\right)\right] \ ,
\end{aligned}$$

$$\begin{aligned}
\beta_g^{(2)} &= 12g_3(t)^2 g(t)^3 + \left(\frac{35}{6}g(t)^2 + \frac{3}{2}g'(t)^2 - \frac{3}{2}h_t(t)^2\right)g(t)^3 \ , \\
\beta_{g'}^{(2)} &= \frac{44}{3}g_3(t)^2 g'(t)^3 + \left(\frac{9}{2}g(t)^2 + \frac{199}{18}g'(t)^2 - \frac{17}{6}h_t(t)^2\right)g'(t)^3 \ , \\
\beta_{g_3}^{(2)} &= g_3(t)^3\left(\frac{9}{2}g(t)^2 - 26g_3(t)^2 + \frac{11}{6}g'(t)^2 - 2h_t(t)^2\right) \ .
\end{aligned}$$

The leading terms in the 3-loop β-functions of λ and h_t are [12]:

$$\begin{aligned}
\beta_\lambda^{(3)} &= 12\Big[(-\frac{266}{3}+32\zeta_3)g_3(t)^4h_t(t)^4+(-38+240\zeta_3)g_3(t)^2h_t(t)^6-(\frac{1599}{8}+36\zeta_3)h_t(t)^8 \\
&+\frac{1}{6}(\frac{1244}{3}-48\zeta_3)g_3(t)^4h_t(t)^2\lambda(t)+\frac{1}{6}(895-1296\zeta_3)g_3(t)^2h_t(t)^4\lambda(t)+ \\
&\frac{1}{6}(\frac{117}{8}-198\zeta_3)h_t(t)^6\lambda(t)+\frac{1}{36}(-1224+1152\zeta_3)g_3(t)^2h_t(t)^2\lambda(t)^2+ \\
&\frac{1}{36}(\frac{1719}{2}+756\zeta_3)h_t(t)^4\lambda(t)^2+\frac{97}{24}h_t(t)^2\lambda(t)^3+\frac{1}{1296}(3588+2016\zeta_3)\lambda(t)^4\Big]\,, \\
\beta_{h_t}^{(3)} &= 2\Big[(-\frac{2083}{3}+320\zeta_3)g_3(t)^6+(\frac{3827}{12}-114\zeta_3)g_3(t)^4h_t(t)^2-\frac{157}{2}g_3(t)^2h_t(t)^4 \\
&+(\frac{339}{16}+\frac{27}{4}\zeta_3)h(t)^6+\frac{4}{3}g_3(t)^2h_t(t)^2\lambda(t)+\frac{33}{2}h_t(t)^4\lambda(t)+\frac{5}{96}h_t(t)^2\lambda(t)^2-\frac{1}{12}\lambda(t)^3\Big]\,,
\end{aligned}$$

where $\zeta_3 = 1.20206...$ is the Riemann zeta function.

The complete 3-loop β-functions for the gauge couplings are [11]:

$$\begin{aligned}
\beta_g^{(3)} &= \frac{324953}{1728}g(t)^7+39g(t)^5g_3(t)^2+81g(t)^3g_3(t)^4+\frac{291}{32}g(t)^5g'(t)^2-\frac{1}{3}g(t)^3g_3(t)^2g'(t)^2 \\
&-\frac{5597}{576}g(t)^3g'(t)^4-\frac{729}{32}g(t)^5h_t(t)^2-7g(t)^3g_3(t)^2h_t(t)^2-\frac{593}{96}g(t)^3g'(t)^2h_t(t)^2 \\
&+\frac{147}{16}g(t)^3h_t(t)^4\,, \\
\beta_{g'}^{(3)} &= \frac{1315}{64}g(t)^4g'(t)^3-g(t)^2g_3(t)^2g'(t)^3+99g_3(t)^4g'(t0^3+\frac{205}{96}g(t)^2g'(t)^5-\frac{137}{27}g_3(t)^2g'(t)^5 \\
&-\frac{388613}{5184}g'(t)^7-\frac{785}{32}g(t)^2g'(t)^3h_t(t)^2-\frac{29}{3}g_3(t)^2g'(t)^3h_t(t)^2-\frac{2827}{288}g'(t)^5h_t(t)^2 \\
&+\frac{315}{16}g'(t)^3h_t(t)^4\,, \\
\beta_{g_3}^{(3)} &= \frac{109}{8}g(t)^4g_3(t)^3+21g(t)^2g_3(t)^5+\frac{65}{2}g_3(t)^7-\frac{1}{8}g(t)^2g_3(t)^3g'(t)^2+\frac{77}{9}g_3(t)^5g'(t)^2 \\
&-\frac{2615}{216}g_3(t)^3g'(t)^4-\frac{93}{8}g(t)^2g_3(t)^3h_t(t)^2-40g_3(t)^5h_t(t)^2+\frac{101}{24}g_3(t)^3g'(t)^2h_t(t)^2 \\
&+15g_3(t)^3h_t(t)^4\,.
\end{aligned}$$

2. Higgs quartic coupling matching

According to Sirlin and Zucchini [27], the 1-loop matching is given by

$$\delta_H^{(1)}(\mu) = \frac{G_\mu m_Z^2}{8\sqrt{2}\pi^2}\left(\xi f_1(\mu)+f_0(\mu)+\frac{f_{-1}(\mu)}{\xi}\right)\,, \tag{A1}$$

where $\xi = \frac{m_H^2}{m_Z^2}$ and, introducing $c = \frac{m_W}{m_Z}$,

$$f_1(\mu) = \frac{3}{2}\log(\xi) - \log\left(c^2\right) + 6\log\left(\frac{\mu^2}{m_H^2}\right) - \frac{1}{2}Z\left[\frac{1}{\xi}\right] - Z\left[\frac{c^2}{\xi}\right] + \frac{9}{2}\left(\frac{25}{9} - \frac{\pi}{\sqrt{3}}\right) \quad \text{(A2)}$$

$$f_0(\mu) = \frac{3c^2}{s^2}\log\left(c^2\right) + 12\log c^2\left(c^2\right) + \frac{3\xi c^2}{\xi - c^2}\log\left(\frac{\xi}{c^2}\right) + 4c^2\, Z\left[\frac{c^2}{\xi}\right] - \frac{15}{2}\left(2c^2 + 1\right) \quad \text{(A3)}$$

$$-6\left(2c^2 - \frac{2m_t^2}{m_Z^2} + 1\right)\log\left(\frac{\mu^2}{m_Z^2}\right) - \frac{3m_t^2}{m_Z^2}\left(4\log\left(\frac{m_t^2}{m_Z^2}\right) + 2\, Z\left[\frac{m_t^2}{m_Z^2\xi}\right] - 5\right)$$

$$+2\, Z\left[\frac{1}{\xi}\right], \quad \text{(A4)}$$

$$f_{-1}(\mu) = 8\left(2c^4 + 1\right) - 12c^4\log\left(c^2\right) - 12c^4\, Z\left[\frac{c^2}{\xi}\right] + 6\left(2c^4 - \frac{4m_t^4}{m_Z^4} + 1\right)\log\left(\frac{\mu^2}{m_Z^2}\right)$$

$$-6\, Z\left[\frac{1}{\xi}\right] + \frac{24m_t^4}{m_Z^4}\left(\log\left(\frac{m_t^2}{m_Z^2}\right) + Z\left[\frac{m_t^2}{m_Z^2\xi}\right] - 2\right), \quad \text{(A5)}$$

$$Z[z] = \begin{cases} 2A(z)\arctan\left(\frac{1}{A(z)}\right) & \text{if } z > \frac{1}{4} \\ A(z)\log\left(\frac{A(z)+1}{1-A(z)}\right) & \text{if } z < \frac{1}{4} \end{cases}, \quad \text{(A6)}$$

$$A(z) = \sqrt{|1 - 4z|}\,. \quad \text{(A7)}$$

We compute the QCD and the Yukawa contribution to $\lambda^{(2)}(\mu)$ following the expressions of [14] (multiplied them by a factor of 6 to compensate for the different definition of the quartic coupling).

Appendix B: Seesaw contribution to the β-functions

Below the right handed neutrino mass scale, the running of the effective light Majorana neutrino mass is given by [49]

$$\frac{dm_\nu(t)}{dt} = \kappa\left(-3g_2(t)^2 + 6h_t(t)^2 + \frac{\lambda(t)}{6}\right)m_\nu(t)\,. \quad \text{(B1)}$$

For $\mu > M_\nu$, we have [50]

$$\frac{dh_\nu(t)}{dt} = \kappa\, h_\nu(t)\left(\frac{5}{4}h_\nu(t)^2 + \frac{3}{2}h_t(t)^2 - \frac{3}{4}g'(t)^2 - \frac{9}{4}g(t)^2\right), \quad \text{(B2)}$$

together with

$$\delta\beta_\lambda^{(1)} = -3h_\nu(t)^4 + 2\lambda(t)h_\nu(t)^2\,, \quad \delta\beta_{h_t}^{(1)} = \frac{1}{2}h_\nu(t)^2\,. \quad \text{(B3)}$$

[1] G. Aad *et al.* [ATLAS Collaboration], Phys. Lett. B [arXiv:1207.7214 [hep-ex]].

[2] S. Chatrchyan *et al.* [CMS Collaboration], Phys. Lett. B [arXiv:1207.7235 [hep-ex]].

[3] P. Q. Hung, Phys. Rev. Lett. **42** (1979) 873. N. Cabibbo, L. Maiani, G. Parisi and R. Petronzio, Nucl. Phys. B **158** (1979) 295. M. Lindner, Z. Phys. C **31** (1986) 295. M. Lindner, M. Sher and H. W. Zaglauer, Phys. Lett. B **228** (1989) 139. M. Sher, Phys. Rept. **179** (1989) 273. M. Sher, Phys. Lett. B **317**, 159 (1993) [Addendum-ibid. B **331**, 448 (1994)] [arXiv:hep-ph/9307342]. G. Altarelli and G. Isidori, Phys. Lett. B **337**, 141 (1994). C. D. Froggatt and H. B. Nielsen, Phys. Lett. B **368** (1996) 96 [hep-ph/9511371]. B. Schrempp and M. Wimmer, Prog. Part. Nucl. Phys. **37** (1996) 1 [hep-ph/9606386].

[4] J. A. Casas, J. R. Espinosa and M. Quiros, Phys. Lett. B **342**, 171 (1995) [arXiv:hep-ph/9409458]. J. R. Espinosa and M. Quiros, Phys. Lett. B **353**, 257 (1995) [arXiv:hep-ph/9504241]. J. A. Casas, J. R. Espinosa and M. Quiros, Phys. Lett. B **382** (1996) 374 [hep-ph/9603227].

[5] G. Isidori, G. Ridolfi and A. Strumia, Nucl. Phys. B **609** (2001) 387 [hep-ph/0104016]. J. R. Espinosa, G. F. Giudice and A. Riotto, JCAP **0805** (2008) 002 [arXiv:0710.2484 [hep-ph]]. G. Isidori, V. S. Rychkov, A. Strumia and N. Tetradis, Phys. Rev. D **77** (2008) 025034 [arXiv:0712.0242 [hep-ph]]. N. Arkani-Hamed, S. Dubovsky, L. Senatore and G. Villadoro, JHEP **0803** (2008) 075 [arXiv:0801.2399 [hep-ph]]. J. Ellis, J. R. Espinosa, G. F. Giudice, A. Hoecker and A. Riotto, Phys. Lett. B **679** (2009) 369 [arXiv:0906.0954 [hep-ph]].

[6] M. Holthausen, K. S. Lim and M. Lindner, JHEP **1202** (2012) 037 [arXiv:1112.2415 [hep-ph]].

[7] I. Masina and A. Notari, Phys. Rev. D **85** (2012) 123506 [arXiv:1112.2659 [hep-ph]].

[8] J. Elias-Miro, J. R. Espinosa, G. F. Giudice, G. Isidori, A. Riotto and A. Strumia, Phys. Lett. B **709** (2012) 222 [arXiv:1112.3022 [hep-ph]].

[9] Z. -z. Xing, H. Zhang and S. Zhou, Phys. Rev. D **86** (2012) 013013 [arXiv:1112.3112 [hep-ph]].

[10] ATLAS Collaboration, Phys. Lett. B **710**, 49 (2012); Phys. Rev. Lett. **108**, 111803 (2012); arXiv:1202.1415 [hep-ex]. CMS Collaboration, arXiv:1202.1488 [hep-ex].

[11] L. N. Mihaila, J. Salomon and M. Steinhauser, Phys. Rev. Lett. **108** (2012) 151602 [arXiv:1201.5868 [hep-ph]].

[12] K. G. Chetyrkin and M. F. Zoller, JHEP **1206** (2012) 033 [arXiv:1205.2892 [hep-ph]].

[13] F. Bezrukov, M. Y. Kalmykov, B. A. Kniehl and M. Shaposhnikov, arXiv:1205.2893 [hep-ph].

[14] G. Degrassi, S. Di Vita, J. Elias-Miro, J. R. Espinosa, G. F. Giudice, G. Isidori and A. Strumia, JHEP **1208** (2012) 098 [arXiv:1205.6497 [hep-ph]].

[15] S. Alekhin, A. Djouadi and S. Moch, arXiv:1207.0980 [hep-ph].

[16] [Tevatron Electroweak Working Group and CDF and D0 Collaborations], arXiv:1107.5255 [hep-ex].

[17] I. Masina and A. Notari, Phys. Rev. Lett. **108** (2012) 191302 [arXiv:1112.5430 [hep-ph]].

[18] I. Masina and A. Notari, arXiv:1204.4155 [hep-ph].

[19] J. Beringer et al. (Particle Data Group), "Review of particle physics", Phys. Rev. D86, 010001 (2012)

[20] C. Ford, D. R. T. Jones, P. W. Stephenson and M. B. Einhorn, Nucl. Phys. B **395**, 17 (1993) [arXiv:hep-lat/9210033]; C. Ford, I. Jack and D. R. T. Jones, Nucl. Phys. B 387 (1992) 373 [Erratum-ibid. B 504 (1997) 551] [arXiv:hep-ph/0111190].

[21] D. J. Gross and F. Wilczek, Phys. Rev. Lett. **30** (1973) 1343. D. J. Gross and F. Wilczek, Phys. Rev. D **8** (1973) 3633. H. D. Politzer, Phys. Rev. Lett. **30** (1973) 1346. D. R. T. Jones, Nucl. Phys. B **75** (1974) 531. W. E. Caswell, Phys. Rev. Lett. **33** (1974) 244.

[22] O. V. Tarasov and A. A. Vladimirov, Sov. J. Nucl. Phys. **25** (1977) 585 [Yad. Fiz. **25** (1977) 1104]. O. V. Tarasov, A. A. Vladimirov and A. Y. Zharkov, Phys. Lett. B **93**, 429 (1980); D. R. T. Jones, M. Fischler and J. Oliensis, Phys. Lett. B **119** (1982) 385. M. E. Machacek and M. T. Vaughn, Nucl. Phys. B **222** (1983) 83. M. E. Machacek and M. T. Vaughn, Nucl. Phys. B **236** (1984) 221. M. E. Machacek and M. T. Vaughn, Nucl. Phys. B **249** (1985) 70.

[23] S. A. Larin and J. A. M. Vermaseren, Phys. Lett. B **303**, 334 (1993) [arXiv:hep-ph/9302208].

[24] T. van Ritbergen, J. A. M. Vermaseren and S. A. Larin, Phys. Lett. B **400**, 379 (1997) [arXiv:hep-ph/9701390].

[25] M. -x. Luo and Y. Xiao, Phys. Rev. Lett. **90** (2003) 011601 [hep-ph/0207271].

[26] M. Czakon, Nucl. Phys. B **710**, 485 (2005) [arXiv:hep-ph/0411261].

[27] A. Sirlin and R. Zucchini, Nucl. Phys. B **266**, 389 (1986).

[28] R. Hempfling and B. A. Kniehl, Phys. Rev. D **51**, 1386 (1995) [arXiv:hep-ph/9408313].

[29] K. G. Chetyrkin and M. Steinhauser, Nucl. Phys. B **573** (2000) 617 [hep-ph/9911434].

[30] N. Gray, D. J. Broadhurst, W. Grafe and K. Schilcher, Z. Phys. C **48**, 673 (1990).

[31] D. J. Broadhurst, N. Gray and K. Schilcher, Z. Phys. C **52**, 111 (1991).

[32] J. Fleischer, F. Jegerlehner, O. V. Tarasov and O. L. Veretin, Nucl. Phys. B **539**, 671 (1999) [Erratum-ibid. B **571**, 511 (2000)] [arXiv:hep-ph/9803493].

[33] K. Melnikov and T. v. Ritbergen, Phys. Lett. B **482** (2000) 99 [hep-ph/9912391].

[34] F. Jegerlehner and M. Y. Kalmykov, Nucl. Phys. B **676**, 365 (2004) [arXiv:hep-ph/0308216].

[35] G. Aad *et al.* [ATLAS Collaboration], arXiv:0901.0512 [hep-ex]. G. L. Bayatian *et al.* [CMS Collaboration], J. Phys. G G **34** (2007) 995.

[36] M. Shaposhnikov and C. Wetterich, Phys. Lett. B **683** (2010) 196 [arXiv:0912.0208 [hep-th]].

[37] E. Komatsu *et al.* [WMAP Collaboration], Astrophys. J. Suppl. **192** (2011) 18 [arXiv:1001.4538 [astro-ph.CO]].

[38] [Planck Collaboration], astro-ph/0604069. See also: C. Burigana, C. Destri, H. J. de Vega, A. Gruppuso, N. Mandolesi, P. Natoli and N. G. Sanchez, Astrophys. J. **724** (2010) 588 [arXiv:1003.6108 [astro-ph.CO]].

[39] J. Bock *et al.* [EPIC Collaboration], arXiv:0906.1188 [astro-ph.CO].

[40] F. R. Bouchet *et al.* [COrE Collaboration], arXiv:1102.2181 [astro-ph.CO].

[41] J. A. Casas, V. Di Clemente, A. Ibarra and M. Quiros, Phys. Rev. D **62** (2000) 053005 [hep-ph/9904295].

[42] I. Gogoladze, N. Okada and Q. Shafi, Phys. Lett. B **668** (2008) 121 [arXiv:0805.2129 [hep-ph]].

[43] W. Rodejohann and H. Zhang, JHEP **1206** (2012) 022 [arXiv:1203.3825 [hep-ph]].

[44] J. Chakrabortty, M. Das and S. Mohanty, arXiv:1207.2027 [hep-ph].

[45] S. Davidson and A. Ibarra, Phys. Lett. B **535** (2002) 25 [hep-ph/0202239].

[46] J. Elias-Miro, J. R. Espinosa, G. F. Giudice, H. M. Lee and A. Strumia, JHEP **1206** (2012) 031 [arXiv:1203.0237 [hep-ph]]. See also: L. Basso, S. Moretti and G. M. Pruna, Phys. Rev. D **82** (2010) 055018 [arXiv:1004.3039 [hep-ph]].

[47] O. Lebedev, Eur. Phys. J. C **72** (2012) 2058 [arXiv:1203.0156 [hep-ph]].

[48] F. L. Bezrukov and M. Shaposhnikov, Phys. Lett. B **659** (2008) 703 [arXiv:0710.3755 [hep-th]]. F. Bezrukov and M. Shaposhnikov, JHEP **0907** (2009) 089 [arXiv:0904.1537 [hep-ph]]. F. Bezrukov, D. Gorbunov and M. Shaposhnikov, JCAP **1110** (2011) 001 [arXiv:1106.5019 [hep-ph]].

[49] K. S. Babu, C. N. Leung and J. T. Pantaleone, Phys. Lett. B **319** (1993) 191 [hep-ph/9309223].

[50] Y. F. Pirogov and O. V. Zenin, Eur. Phys. J. C **10** (1999) 629 [hep-ph/9808396].